Affinity purification mass spectrometry analysis of PD-1 uncovers SAP as a new checkpoint inhibitor

Michael Peled[a], Anna S. Tocheva[a], Sabina Sandigursky[a], Shruti Nayak[b], Elliot A. Philips[c], Kim E. Nichols[d], Marianne Strazza[a], Inbar Azoulay-Alfaguter[a], Manor Askenazi[e], Benjamin G. Neel[f], Adam J. Pelzek[a], Beatrix Ueberheide[b,f], and Adam Mor[a,f,1]

[a]Department of Medicine, New York University School of Medicine, New York, NY 10016; [b]Proteomics Laboratory, Division of Advanced Research Technologies, New York University School of Medicine, New York, NY 10016; [c]Department of Biochemistry and Molecular Pharmacology, New York University School of Medicine, New York, NY 10016; [d]Department of Oncology, St. Jude Children's Research Hospital, Memphis, TN 38105; [e]Biomedical Hosting LLC, Arlington, MA 02474; and [f]Perlmutter Cancer Center, New York University School of Medicine, New York, NY 10016

Edited by Rafi Ahmed, Emory University, Atlanta, GA, and approved December 5, 2017 (received for review June 9, 2017)

Programmed cell death-1 (PD-1) is an essential inhibitory receptor in T cells. Antibodies targeting PD-1 elicit durable clinical responses in patients with multiple tumor indications. Nevertheless, a significant proportion of patients do not respond to anti–PD-1 treatment, and a better understanding of the signaling pathways downstream of PD-1 could provide biomarkers for those whose tumors respond and new therapeutic approaches for those whose tumors do not. We used affinity purification mass spectrometry to uncover multiple proteins associated with PD-1. Among these proteins, signaling lymphocytic activation molecule-associated protein (SAP) was functionally and mechanistically analyzed for its contribution to PD-1 inhibitory responses. Silencing of SAP augmented and overexpression blocked PD-1 function. T cells from patients with X-linked lymphoproliferative disease (XLP), who lack functional SAP, were hyperresponsive to PD-1 signaling, confirming its inhibitory role downstream of PD-1. Strikingly, signaling downstream of PD-1 in purified T cell subsets did not correlate with PD-1 surface expression but was inversely correlated with intracellular SAP levels. Mechanistically, SAP opposed PD-1 function by acting as a molecular shield of key tyrosine residues that are targets for the tyrosine phosphatase SHP2, which mediates PD-1 inhibitory properties. Our results identify SAP as an inhibitor of PD-1 function and SHP2 as a potential therapeutic target in patients with XLP.

PD-1 | SAP | T cells | SHP2 | XLP

Tight control of T cell activation is essential to maintain immune homeostasis. T cell surface- expressed inhibitory receptors are key regulators that limit excessive T cell responses and in recent years have proven to be important targets for anticancer therapeutics. Programmed cell death-1 (PD-1) is a critical inhibitory receptor, and numerous in vivo and in vitro studies have documented its inhibitory function in T cells. PD-1–knockout mice develop autoimmune manifestations, such as glomerulonephritis and inflammatory cardiomyopathy (1, 2), and PD-1 ligation reduces numerous T cell functions, including proliferation, adhesion, and secretion of cytokines (3–5). Consistent with these observations, engagement of PD-1 also inhibits activation and expansion of effector T cells in infectious and autoimmune models (6–8).

PD-1 is a member of the CD28 receptor extended family (9) and is expressed on activated T and B cells, natural killer cells, monocytes, dendritic cells, and melanoma cells (10–12). There are two PD-1 ligands: PD-1 ligand 1 (PDL1; also known as "B7-H1") (13, 14) and PD-1 ligand 2 (PDL2; also known as "B7-DC") (15, 16). PDL1 is widely expressed in hematopoietic and nonhematopoietic cells, whereas PDL2 is expressed mainly on antigen-presenting cells (APCs). PD-1 has recently drawn attention because of the clinical efficacy of blocking the PD-1 pathway in cancer immunotherapy (17, 18). However, durable responses to anti–PD-1 interventions are limited to a fraction of patients (19), and many develop immune-related adverse events (20). Despite the wide utilization of PD-1–based therapies, the molecular mechanisms underlying its inhibitory effects on lymphocyte function are only partially understood. Live-cell imaging revealed that during T cell activation PD-1 is localized to the immunological synapse (21), where it accumulates with T cell-receptor (TCR) microclusters (22). Subsequently, the tyrosine phosphatase SHP2 [Src homology 2 (SH2) domain containing tyrosine phosphatase 2] is recruited to the cytoplasmic tail of PD-1 and is associated with the dephosphorylation of key tyrosine residues within the CD3 complex, as well as CD28 and the proximal signaling molecules ZAP70, PI3K, AKT, C3G, and ERK (3–5, 23, 24).

The cytoplasmic tail of PD-1 contains two tyrosine motifs, an immunoreceptor tyrosine-based inhibitory motif (ITIM) and an immunoreceptor tyrosine based-switch motif (ITSM) (25). Both motifs are phosphorylated upon PD-1 engagement (24, 25). Mutagenesis studies revealed a primary role for the ITSM in SHP2 recruitment, as opposed to the ITIM, whose role in PD-1 signaling and function is not clear (4). Furthermore, while most coreceptor cytoplasmic tails are shorter than 60 aa (26), the tail of PD-1 consists of 97 aa, suggesting it might interact with additional, yet unknown, proteins. To uncover intracellular proteins that interact with PD-1, we used the PD-1 cytoplasmic tail as a bait to affinity purify candidate proteins in activated human T cells, followed by identification with high-resolution MS. In addition to SHP2, we discovered several other PD-1–interacting partners, including the signaling lymphocytic activation molecule (SLAM)-associated protein (SAP), also known as "SH2D1A"

Significance

Antibodies targeting PD-1 have elicited clinical responses in multiple tumors. Nevertheless, response to anti–PD-1 interventions is limited to a fraction of patients, and a comprehensive understanding of the signaling downstream of PD-1 could provide biomarkers for tumor response. We used affinity purification-mass spectrometry to uncover proteins associated with PD-1 and found that the adaptor protein SAP inhibits PD-1 functions by blocking the enzymatic interaction between the phosphatase SHP2 and the subset of its substrates that also bind to SAP. Signaling downstream of PD-1 in T cell subsets did not correlate with PD-1 expression but was inversely correlated with SAP levels. Thus, SAP is a modulator of PD-1 function and a potential biomarker for reduced responses to PD-1–based interventions.

Author contributions: M.P., A.S.T., E.A.P., M.S., I.A.-A., B.G.N., A.J.P., B.U., and A.M. designed research; M.P., A.S.T., S.S., S.N., M.A., B.U., and A.M. performed research; K.E.N., M.A., and A.M. contributed new reagents/analytic tools; M.P., A.S.T., S.N., E.A.P., K.E.N., M.S., B.G.N., A.J.P., B.U., and A.M. analyzed data; and M.P. and A.M. wrote the paper.

The authors declare no conflict of interest.

This article is a PNAS Direct Submission.

[1]To whom correspondence should be addressed. Email: Adam.Mor@NYUMC.org.

This article contains supporting information online at www.pnas.org/lookup/suppl/doi:10.1073/pnas.1710437115/-/DCSupplemental.

(SH2 domain-containing protein 1A). Interestingly, SAP blocked PD-1 inhibitory functions in T cells (such as adhesion, proliferation, and cytokine secretion) through indirect inhibition of SHP2 activity. Accordingly, interventions at the level of the PD-1/SAP pathway might provide a novel mechanism to enhance T cell responses and thus optimize the treatment of malignancies, immunodeficiencies, and chronic infections.

Results

MS-Based Approach Identifies PD-1–Interacting Proteins. The identification of proteins associated with transmembrane receptors by affinity purification can be challenging due to the extraction conditions needed to solubilize receptors, to which the relevant complexes are labile (27). To overcome this limitation, we utilized GST-tagged versions of the PD-1 cytoplasmic tail (97 aa long) to affinity purify intracellular proteins from lysates of Jurkat T cells (Fig. 1*A*). To differentiate between phosphotyrosine-dependent and independent interactions, we used an unmodified (WT) PD-1 tail, a phosphodeficient version in which the tyrosine residues were replaced by phenylalanines (Y223F and Y248F), or a phosphomimetic version in which both tyrosine residues were replaced by glutamic acid (Y223E and Y248E) to serve as baits for PD-1–interacting proteins. The GST–PD-1 tails were mixed with lysates from activated T cells, and associated proteins were identified by MS. Label-free relative quantitative analysis using spectral counts was performed to determine the amount of each protein that interacted with the respective GST fusion proteins. SHP2 is the only protein reported to interact strongly with the tail of PD-1. As expected, based on the phosphotyrosine dependence of the SHP2/PD1 interaction, although each bait was present in similar amounts in the various experimental conditions (Fig. 1*B*), it was mainly the GST–PD-1 WT version that pulled down the highest amount of SHP2 (Fig. 1 *C* and *D*). Since the Y223E, Y248E version of PD-1 demonstrated inferior binding to SHP2 compared with the WT protein, we excluded this condition from our MS analysis. Western blot analysis confirmed that the pulled down GST—PD-1 WT was phosphorylated after mixing with the cell lysate (Fig. S1), and the MS analysis also confirmed that WT PD-1 was phosphorylated (Dataset S1). Therefore, the WT version of the tail of PD-1 could reliably serve as a proxy for the activated PD-1.

To identify PD-1 tail-specific interactions, we excluded proteins that were affinity-purified by the GST protein itself (GST control) (Fig. 1*E*). Proteins that were affinity-purified by GST–PD-1 Y223F, Y248F were designated as PD-1 tyrosine-independent candidates (182 candidates) (Fig. 1*E* and Dataset S2). Proteins that were detected only by the GST–PD-1 WT baits were regarded as potential tyrosine-specific interactors (38 candidates) (Fig. 1*E* and Dataset S3). Importantly, SHP2, the only protein known to interact with the tail of PD-1, was affinity-purified by all three replicates of the GST–PD-1 WT but not by GST alone or by the GST–PD-1 Y223F, Y248F tails.

We next sought to identify additional proteins that were preferentially affinity-purified by GST–PD-1 WT over GST–PD-1 Y223F, Y248F. Because the phosphorylated tyrosine residues of PD-1 are part of the ITIM and ITSM that interact preferentially with SH2 domains, we sorted our candidate interactors into proteins containing SH2 domains (UniProt) (Fig. 1*F* and Table 1). Based on the cellular expression and the function of PD-1, we further narrowed our considerations to proteins that were annotated as immune-related according to the Mouse Genome Informatics database, which contains annotations of the phenotypes of knockout mice (Fig. 1*F* and Table 1). Accordingly, 13 PD-1–binding proteins were identified (Table 1). SHP2 demonstrated the highest binding selectivity toward WT baits, recapitulating previous observations of SHP2 interaction with the ITSM of PD-1 (Fig. 1*F*). Interestingly, STRING analysis (28) revealed that some of the proteins could interact indirectly with PD-1 through SHP2 (PTPN11) (Fig. 1*G*). We also observed that the adaptor protein SAP was preferentially associated with WT PD-1.

The ITIM of PD-1 Is Necessary for SHP2 Activity. While the contribution of the ITSM of PD-1 to SHP2 binding and downstream signaling is established, the role of the ITIM in PD-1 function is less clear. Because SHP2 has two SH2 domains and could thus potentially bind to two sequential phosphotyrosines (one tyrosine in the PD-1 ITSM and the other tyrosine in the PD-1 ITIM), we hypothesized that the ITIM of PD-1 might facilitate PD-1 signaling by stabilizing SHP2 in an open conformational state (29, 30). To test this possibility, we expressed GFP–PD-1 WT, GFP–PD-1 Y223F (ITIM mutant), or GFP–PD-1 Y248F (ITSM mutant) in cells that were then treated with pervanadate (a diagram describing the experiment is provided in Fig. S2). Next, we combined the phosphorylated GFP–PD-1 proteins obtained by GFP immunoprecipitation with lysates from cells overexpressing SHP2 and recorded the levels of SHP2 bound to each version of PD-1 as well as its specific enzymatic activity. As expected, SHP2 failed to bind to PD-1 when the ITSM was mutated (Y248F) (Fig. 2*A*). Notably, the mutant version of the ITIM (Y223F) inhibited SHP2 binding only to a limited extent (Fig. 2*B*). However, the SHP2 phosphatase activity assay, analyzed on the beads that were used for affinity purification of SHP2, revealed that the ITIM and the ITSM were both equally indispensable for the enzymatic activity (Fig. 2*C*). When Jurkat T cells that expressed different versions of GFP-tagged PD-1 were stimulated with magnetic beads coated with anti–CD3+PDL2-Fc for 24 h, both the ITIM and the ITSM were required for PD-1 signaling to inhibit IL-2 (Fig. 2*D*) and IFN-γ (Fig. 2*E*) secretion. Thus, we propose a two-step activation model in which under resting conditions SHP2 is folded in an autoinhibited conformation (Fig. 2*F*, *Left*). Upon binding of a ligand (such as PDL2) to PD-1, SHP2 is recruited to the phosphorylated ITSM (Fig. 2*F*, *Center*, first step). However, the ITIM must also be phosphorylated to unfold SHP2 to its active conformation (Fig. 2*F*, *Right*, second step).

SAP Is Indirectly Associated with PD-1. SAP is a 128-aa protein with a single SH2 domain that interacts with receptors of the SLAM family, through binding to phosphorylated ITSMs (31). Coimmunoprecipitation experiments, in which lysates of Jurkat T cells expressing GFP-tagged PD-1 (or GFP alone) were immunoprecipitated with an anti-GFP antibody, revealed that endogenous SAP is found in the same signaling complex as PD-1 (Fig. 3 A_i and A_{ii}). In addition, overexpressed GFP–PD-1 and SAP-Cherry were found at the same subcellular compartment, at the plasma membrane of activated T cells (Fig. 3 *B* and *C*). Notably, SAP was recruited to the plasma membrane even with TCR activation alone (anti-CD3 stimulation), which is plausible considering that SAP is known to interact with additional membrane proteins, including the CD3ζ chain (31, 32). As mentioned, SAP is known to interact with phosphorylated tyrosines present within the cytoplasmic tails of the SLAM family receptors, where it might compete with SHP2 for binding (33). To test if this was also the case for PD-1, WT or mutant versions of GFP–PD-1 were expressed and immunoprecipitated from activated T cells. Western blot analysis revealed that both SAP and SHP2 were associated with WT GFP–PD-1 and with GFP–PD-1 Y223F but not with GFP–PD-1 Y248F (Fig. 3 D_i–D_{iii}). Thus, it was the PD-1 ITSM, and not the ITIM, that enabled interaction with both SAP and SHP2. Next, we hypothesized that SAP inhibits PD-1 function by competing with SHP2 for binding to the PD-1 tail. To test that, we performed a competitive binding assay in which overexpressed GFP–SAP competed with endogenous SHP2 on binding to GST–PD-1. As shown, SAP overexpression failed to decrease the levels of SHP2 binding to PD-1, ruling out direct competition between SHP2 and SAP on direct binding to PD-1 (Fig. 3 E_i and E_{ii}). In addition, increasing concentrations of recombinant SAP did not interfere

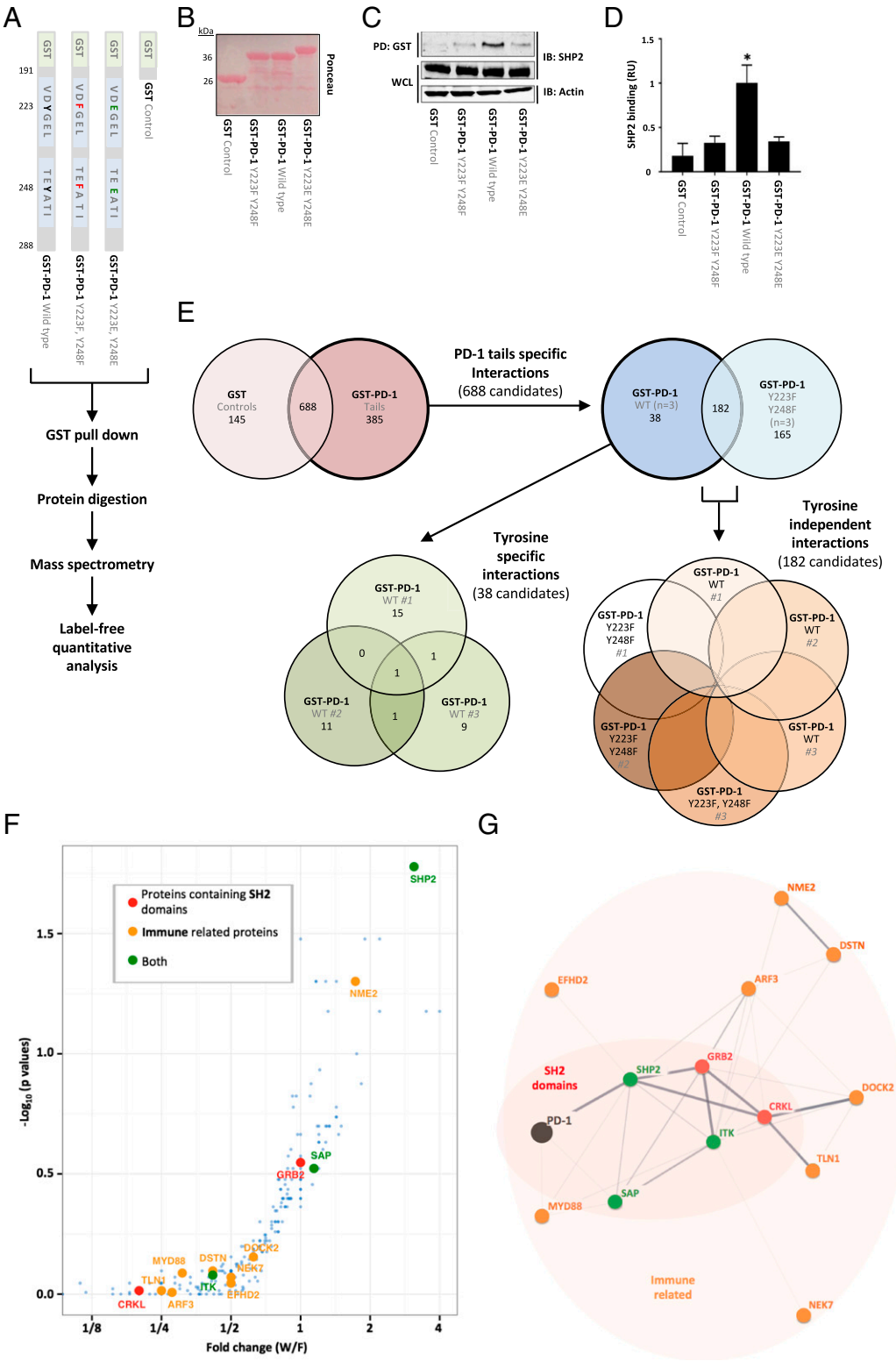

Fig. 1. The MS-based approach identifies PD-1–interacting proteins. (*A*) Experimental design and schematic of the different versions of the GST-tagged PD-1 tails that were used as baits. (*B*) Ponceau staining shows the size and the amount of GST–PD-1 tail fusion protein used in each affinity purification condition. (*C*) Jurkat T cells were activated with pervanadate, and whole-cell lysates (WCL) were used for pull-down (PD) with the GST-tagged baits. Samples were analyzed by immunoblotting (IB), as indicated. (*D*) Densitometry values of the affinity-purified SHP2 after normalization to GST expression levels. All values are fold-change compared with the intensity of SHP2 in the GST–PD-1 WT. Data are presented as mean ± SEM. The asterisk represents a significant difference between the denoted protein and the GST control ($P < 0.05$, unpaired *t* test); $n = 3$. (*E*) Summary of the workflow and the results of pull-down MS analysis. (*F*) One-sided volcano plot of the PD-1 tail-interacting proteins. SH2 domain-containing proteins are highlighted in red; proteins that are highlighted in orange were annotated as immune-related. Proteins labeled in green met both conditions. (*G*) STRING interaction map of PD-1 and the candidate proteins identified. The line thickness indicates the strength of data supporting interaction.

Table 1. Tyrosine-dependent and independent protein interactions of the PD-1 tail

Gene	UniProt ID	Immune related	SH2 domains	Peptide spectrum match
SHP2 (*PTPN11*)	Q06124	+	+	35
ITK	Q08881	+	+	15
SAP (*SH2D1A*)	O60880	+	+	15
EFHD2	Q96C19	+	−	38
ARF3	P61204	+	−	21
DOCK2	Q92608	+	−	13
NME2	P22392	+	−	27
NEK7	Q8TDX7	+	−	13
DSTN	P60981	+	−	17
TLN1	Q9Y490	+	−	10
MYD88	Q99836	+	−	17
GRB2	P62993	−	+	8
CRKL	P46109	−	+	12

A list of the proteins found in the analysis. Peptide spectrum matches are the total number of identified peptide sequences for the protein, including those redundantly identified, in all the baits (excluding GST-only control).

with the affinity purification of SHP2 by GST–PD-1 (Fig. 3 F_i and F_{ii}). To test the possibility that SAP was associated with PD-1 indirectly via its association with SHP2, we knocked down SHP2 in Jurkat T cells and observed that SAP completely failed to bind to PD-1 (Fig. 3 G_i–G_{iii}). These findings suggest that SAP is associated with PD-1 indirectly, possibly through a complex with SHP2 and other adaptor proteins. Notably, the ability of SAP to bind to FYN (34) was not necessary for its ability to inhibit PD-1 signaling and IL-2 secretion (Fig. S3) because a mutant version of SAP (SAP R78A) that cannot bind to FYN could still inhibit PD-1 function.

SHP2 is self-inhibited by its N-terminal SH2 (N-SH2) domain, which folds over its catalytic domain (Fig. 2*F*) (29, 30). SAP and the N-SH2 domain of SHP2 perfectly aligned structurally (Fig. S4), suggesting that SAP might interact with and inhibit the SHP2 catalytic domain directly. To test this possibility, His-tagged SAP and GST-tagged $SHP2^{PTP}$ (the catalytic domain of SHP2) were used in coaffinity enrichment experiments, which showed a lack of direct interaction between these proteins (Fig. 3 H_i and H_{ii}). However, these recombinant proteins were physically associated in the presence of WT T cell (control) lysate (Fig. 3 H_i and H_{ii}), suggesting that additional proteins are required to support the association.

SAP Inhibits SHP2 Activity. Because SAP is known to modulate signaling downstream from several receptors (31, 32), we hypothesized that it also might modulate signaling downstream of PD-1. Indeed, knocking down SAP in Jurkat T cells further enhanced the ability of PD-1 ligation (with PDL2) to inhibit the phosphorylation of ERK, PLCγ, and ZAP70 in CD3-stimulated T cells (Fig. 4*A*, *Left*). Moreover, when SAP-deficient T cells were treated with SHP099, an allosteric specific inhibitor of SHP2 (35), PD-1's ability to inhibit the phosphorylation of ERK, PLCγ, and ZAP70 was abrogated (Fig. 4*A*, *Right* and quantified in Fig. S5). To test if SAP inhibits dephosphorylation of SHP2 substrates, we used a modified phosphatase assay that was based on the in vitro substrate-trapping method (Fig. 4*B* and Fig. S6) (36). As shown, a decrease in the levels of the phosphorylated proteins was recorded with increasing concentration of $SHP2^{PTP}$ (Fig. 4 *B* and *C*). Most importantly, there was an enhanced reduction of total phosphorylation in the SAP-deficient cells (Fig. 4 *B* and *C*), implying that SAP inhibits SHP2-specific activity.

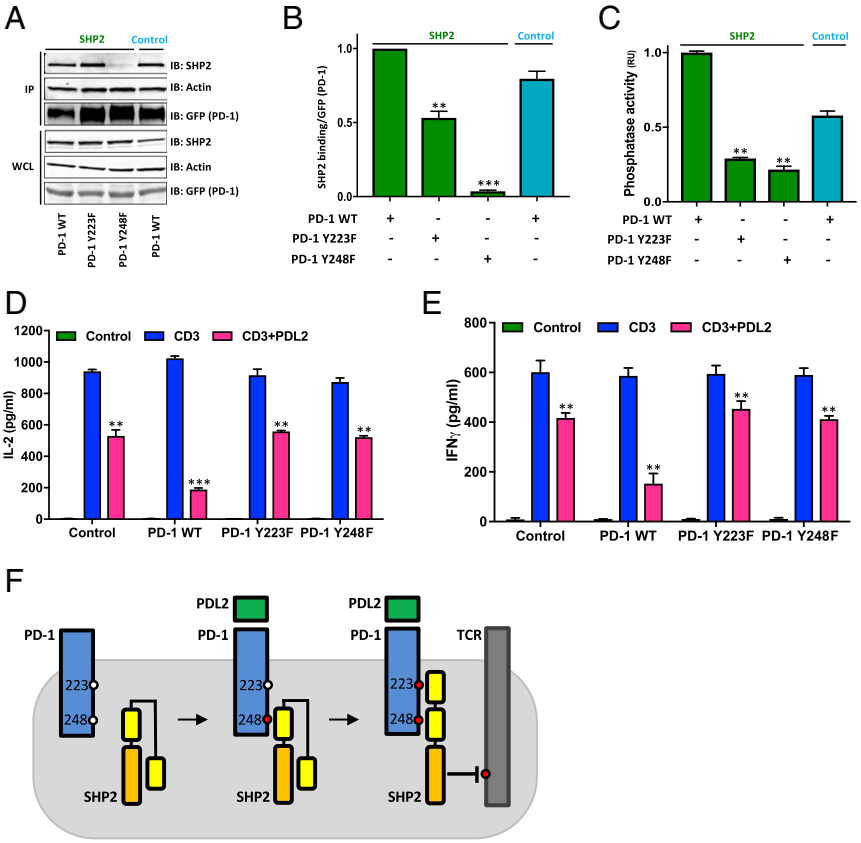

Fig. 2. The ITIM of PD-1 is necessary for SHP2 activity. (*A*–*C*) 293T cells were transfected with the indicated versions of GFP-tagged PD-1, followed by pervanadate treatment and immunoprecipitation using anti-GFP mAb-agarose (*A*). SHP2 levels bound to precipitated GFP-PD-1 were quantified (*B*) and subjected to phosphatase activity assay (*C*). Values of pulled-down SHP2 were normalized to GFP expression levels. All values are fold-change compared with the intensity of precipitated SHP2 in the WT PD-1 GFP in the SHP2-expressing cells. Phosphatase activity values are fold-change compared with the activity of immunoprecipitated SHP2 in the WT PD-1 GFP from the SHP2-expressing cells. RU, relative units. (*D* and *E*) Jurkat T cells were transfected with GFP control or different versions of GFP-tagged PD-1 as indicated, followed by stimulation with magnetic beads coated with anti-CD3, or anti-CD3+PDL2 for an additional 24 h. Medium was collected for IL-2 and IFN-γ measurements (ELISA). (*F*) The two-step activation model. SHP2 is first recruited to the ITSM (step 1), and only then does the second SH2 bind to the ITIM (step 2), which opens the catalytic domain of SHP2 to the fully active conformation. Data are presented as mean ± SEM. Asterisks represent significant differences between the denoted group and the PD-1 WT in *C* and *D* or between the denoted group and the anti-CD3–treated cells in *E* and *F*; $^{**}P < 0.01$, $^{***}P < 0.001$, unpaired *t* test; $n = 3$.

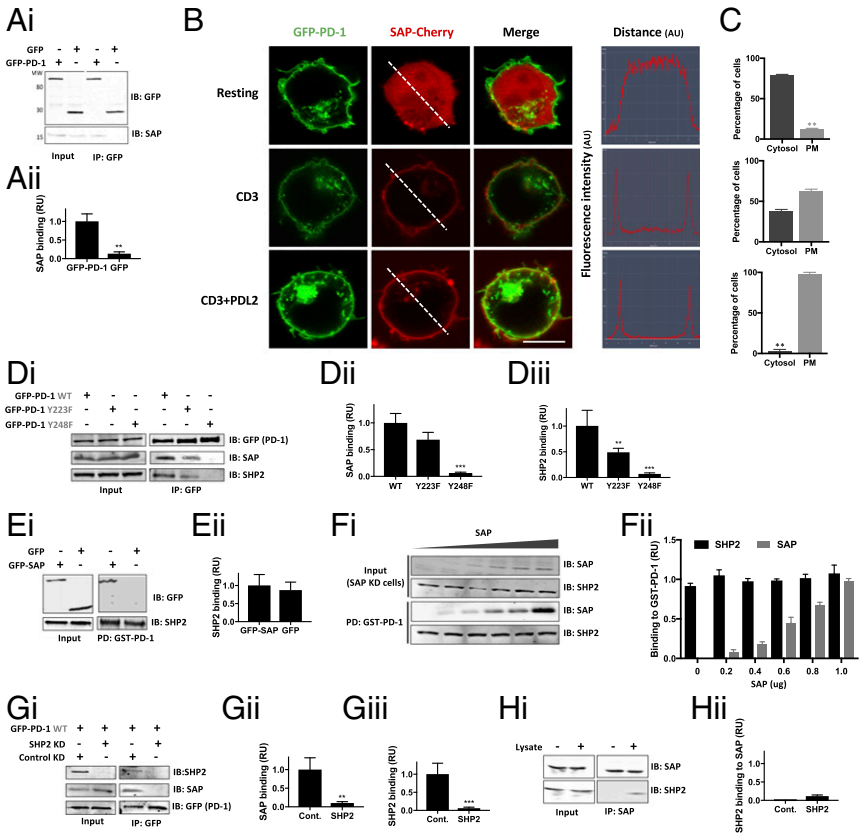

Fig. 3. SAP is indirectly associated with PD-1. (A_i) Pervanadate-treated Jurkat T cells were transiently transfected with GFP-tagged PD-1 or GFP alone. Whole-cell lysates (WCL) were immunoprecipitated with an anti-GFP antibody (IP: GFP), and samples were analyzed by immunoblotting. (A_{ii}) Densitometry values of data shown in A_i. (*B*, *Left*) Jurkat T cells were transfected with plasmids directing the expression of the indicated fluorescent proteins, and after 24 h cells were stimulated with anti-CD3 antibodies and recombinant PDL2, followed by live imaging. (Scale bar, 10 μm.) (*Right*) Line analysis shows fluorescent intensities of SAP (red) along the diameter of the cell. (*C*) Percentage of cells showing SAP localization at the plasma membrane (PM) or the cytosol, in the unstimulated (*Upper*) and stimulated (CD3 or CD3+PDL2) conditions. (D_i) Jurkat T cells were transfected with different versions of GFP-tagged PD-1, as indicated, followed by treatment with pervanadate; whole-cell lysates (Input) were immunoprecipitated with an anti-GFP antibody (IP: GFP), and samples were analyzed by immunoblotting. (D_{ii} and D_{iii}) Densitometry values of data shown in D_i. (E_i) 293T cells were transfected with plasmid directing expression of GFP-SAP or a control GFP plasmid, followed by treatment with pervanadate. Lysates were pulled down with the GST-tagged PD-1, and samples were analyzed by immunoblotting. (E_{ii}) Densitometry values of data shown in E_i. (F_i) increasing concentrations of recombinant SAP were added to SAP knockdown (KD) Jurkat cells followed by affinity purification with GST–PD1 and immunoblot analysis. (F_{ii}) Densitometry values of data shown in F_i. (G_i) SHP2-knockdown and scrambled control Jurkat T cells were transfected with GFP-tagged PD-1, followed by treatment with pervanadate; lysates were immunoprecipitated with an anti-GFP antibody (IP: GFP), and samples were analyzed by immunoblotting. (G_{ii} and G_{iii}) Densitometry values of data shown in G_i. (H_i) His-tagged SAP and GST-tagged SHP2 catalytic domain were incubated in the presence or absence of Jurkat T cell lysate (Control Lysate). SAP was pulled down with nickel beads. Samples were analyzed by immunoblot. (H_{ii}) Densitometry values data shown in H_i. Data are presented as mean ± SEM. Asterisks represent significant differences between the denoted condition and GFP–PD1 WT in *B*, between the denoted condition and the cells with cytosolic distribution of SAP in *C*, and between the denoted condition and the control where only two groups are tested. $*P < 0.05$, $**P < 0.01$, $***P < 0.001$, unpaired *t* test; $n = 3$.

Because SAP inhibits PD-1 signaling (Fig. 4*A*) but does not interfere with SHP2 binding to PD-1 (Fig. 3 *E* and *F*), we considered two alternative mechanisms. First, SAP could bind SHP2 and directly block the SHP2 catalytic site or, alternatively, SAP might not bind to SHP2 but rather could bind to its substrates and thereby block the interaction between SHP2 and its enzymatic substrates. The latter explanation, known as the "shielding model," has been proposed for other signaling complexes (37). In support of this model, we used SHP099 to block SHP2 activity in Jurkat T cells, followed by affinity purification with His-tagged SAP. As expected (Fig. 4*D*), SHP099 treatment resulted in an increase in the levels of select tyrosine phosphorylated proteins (detected by 4G10 antibody). The fact that these SHP2 phosphorylated targets were also affinity-purified by His-tagged SAP indicates that SAP interacts physically with several SHP2 substrates (Fig. 4*D*). To test the effect of SAP on SHP2-mediated dephosphorylation events, we measured SHP2-mediated dephosphorylation of p60-SRC Y416 (Fig. 4*E*), SLAMF5 Y279 (Fig. 4*F*), and CD3 Y142 (Fig. 4*G*) phosphotyrosyl peptides by Malachite Green assays. For these three substrates, and in the absence of SAP, we observed conventional Michaelis–Menten kinetics. However, when we included SAP in the assay, we observed that SHP2-mediated dephosphorylation was inhibited only when the SHP2 substrate was a known SAP interactor (CD3 and SLAMF5 but not p60-SRC) (Fig. 4 *F* and *G*). Consistent with a competitive mechanism of inhibition, K_m values increased two- to threefold in the presence of SAP when phosphorylated SLAMF5 and CD3 peptides were used as substrates but not when p60-SRC peptide was used, whereas V_{max} values were unaffected for all three phosphotyrosyl peptides. The cytoplasmic tail of CD28 was reported to be a significant target for SHP2 downstream of PD-1 (23). To assess if SAP inhibits the dephosphorylation of the tail of CD28, we tested recombinant CD28 Y173, the binding site of lipid kinase PI3K, and recombinant CD28 Y190, the LCK-binding motif (38). Although both sites were targeted by the catalytic domain of SHP2 (Fig. 4 *H* and *I*), SAP predominantly inhibited

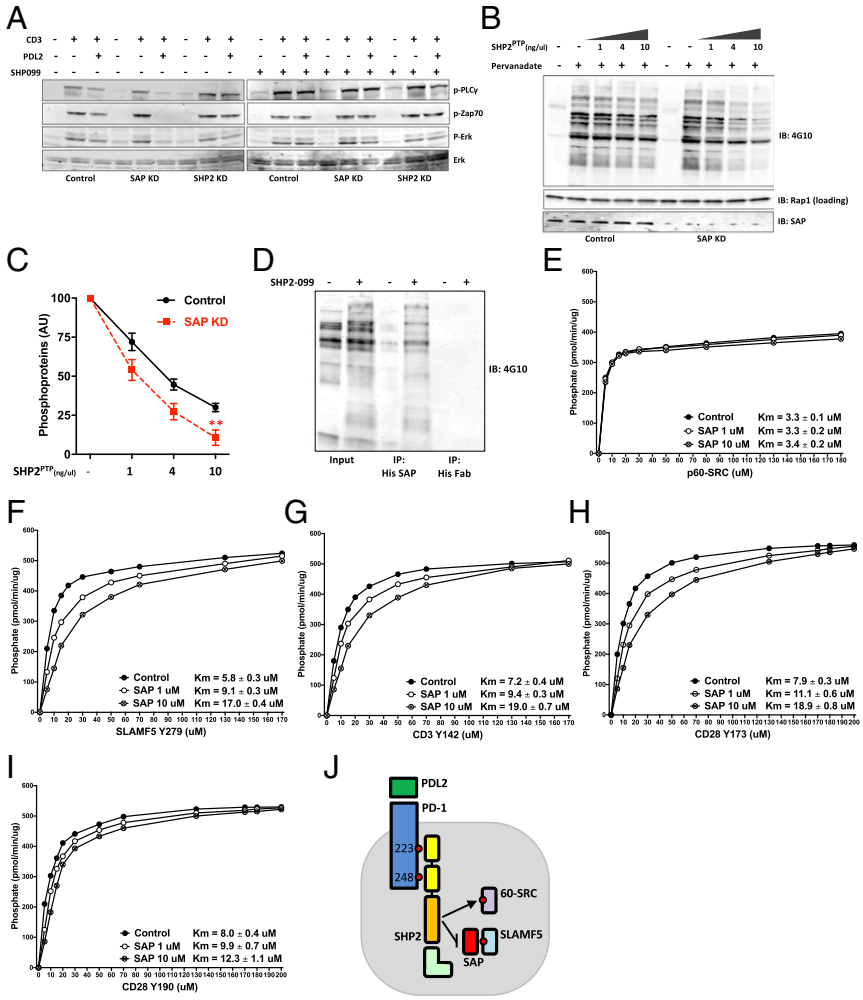

Fig. 4. SAP inhibits SHP2 activity. (*A*) Jurkat T cells stably transfected with shRNA for SAP (SAP KD), SHP2 (SHP2 KD), and nontargeting control (Control) were treated for 1 h with SHP099 (10 uM) followed by stimulation with magnetic beads coated with anti-CD3 or anti-CD3+PDL2 for 5 min. At this time, the cells were harvested and analyzed by immunoblotting, as indicated. (*B*) Jurkat T cells, transfected with siRNA for SAP (SAP KD) and nontargeting control (Control), were treated with pervanadate to induce maximal phosphorylation, followed by five serial washes, lysis, and diafiltration to remove the drug and to exchange the buffer to a phosphatase-compatible buffer. $SHP2^{PTP}$ (the GST-tagged SHP2 catalytic domain) was then added to the cell lysates for 1 h at the indicated concentrations, followed by immunoblotting with anti-phosphotyrosine antibody (antibody clone 4G10). (*C*) Densitometry values of all the phosphotyrosine-containing proteins shown in *B*. All values are relative to the baseline condition (without $SHP2^{PTP}$). (*D*) Jurkat T cells were treated with SHP099 (10 μM), followed by affinity purification with a his-tagged SAP or his-Fab control and immunoblot analysis with anti-phosphotyrosine antibody (4G10). (*E–I*) Enzymatic activity of $SHP2^{PTP}$ was measured using a Malachite Green assay, with p60-SRC (*E*), SLAMF5 Y279 (*F*), CD3 Y142 (*G*), CD28 Y172 (*H*), and CD28 Y190 (*I*) peptides as substrates. Substrate titrations of $SHP2^{PTP}$ (dark circles) at baseline (control) or in the presence of 1 uM SAP (white circles) or 10 uM SAP (crossed circles) are shown. Curves are fitted using the Michelis–Menten equation, and derived K_m values are shown. The data points represent the mean of three measurements. (*J*) A diagram describing the shielding model. Data are presented as mean ± SEM. Asterisks represent significant differences between the denoted group and the anti-CD3–treated cells in *A* or between SAP-deficient cells and control cells in *E*; $*P < 0.05$, $**P < 0.01$, unpaired *t* test; $n = 4$.

dephosphorylation of CD28 Y173 over CD28 Y190. The K_m values for CD28 Y173 were similar to those of CD3 Y142 but were lower than the values for CD28 Y190. Overall, SAP interacts with PD-1 and SHP2 indirectly and inhibits their activity by shielding substrates of SHP2 from its phosphatase activity (Fig. 4*J*).

SAP Inhibits PD-1 Functions. Functionally, knocking down SAP in primary human T cells using siRNA (Fig. S7*A*) further enhanced the ability of PD-1 ligation (with PDL2) to inhibit IL-2 secretion in anti-CD3–stimulated T cells (Fig. 5*A*) and, similar to its effect on PD-1 signaling, treatment with SHP099, resulted in abrogation of PD-1's ability to inhibit IL-2 secretion (Fig. S7*B*). By contrast, overexpression of SAP–GFP (Fig. 5*B* and Fig. S7*C*) abrogated the ability of PD-1 to inhibit anti-CD3–induced IL-2 secretion (Fig. 5*C*), CD69 up-regulation (Fig. 5*D* and Fig. S7*D*), IFN-γ release (Fig. 5*E*), and T cell adhesion to fibronectin-coated wells (Fig. 5*F*). Thus, SAP appears to be a negative regulator of PD-1 signaling and function in T cells.

X-linked lymphoproliferative disease (XLP) is a genetic disease in which the *SH2D1A* gene (which encodes SAP) is mutated, leading to either an absent or a dysfunctional protein (34). XLP patients are immunodeficient and commonly present with dysregulated cellular responses to Epstein–Barr virus infection, which results in excessive lymphoproliferation or hemophagocytic lymphohistiocytosis. To further validate the contribution of SAP to PD-1 signaling, we isolated peripheral T cells from patients with XLP to study the ability of anti-CD3 and +PDL2-Fc–coated beads to modulate cytokine secretion. Compared with healthy control T cells, PD-1 ligation in XLP cells resulted in more profound reduction of IL-2 secretion (Fig. 5*G*). PD-1 ligation also had a more pronounced inhibitory effect on cellular proliferation in XLP cells than in cells from healthy controls (Fig. 5*H*), strongly

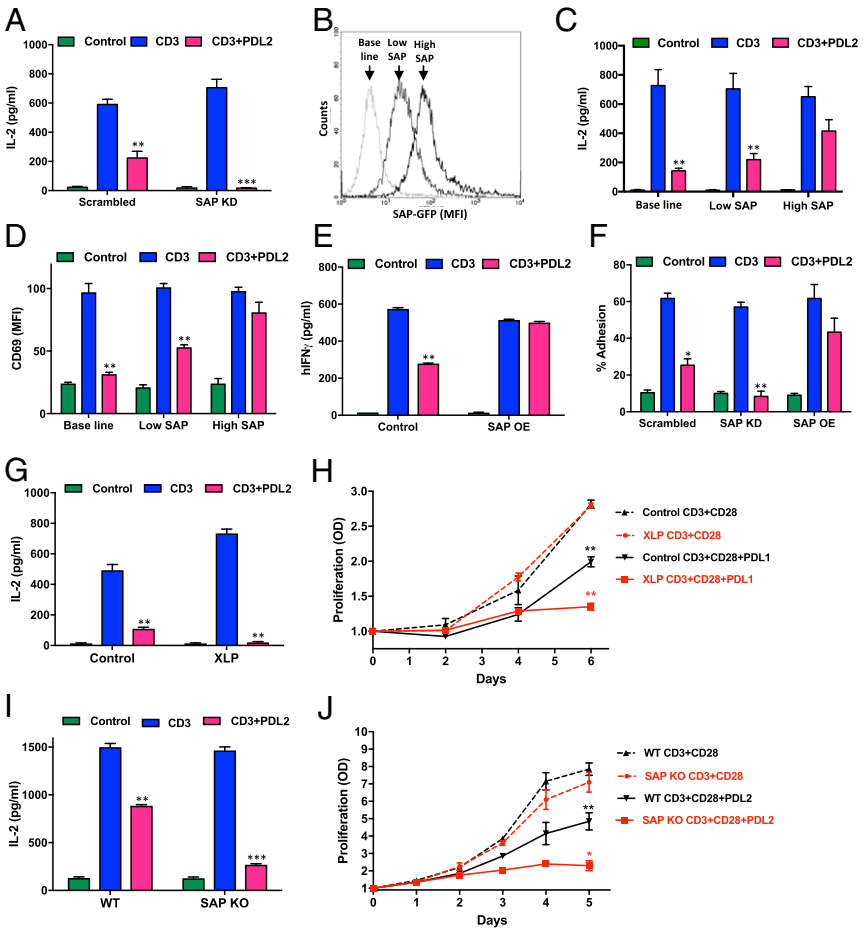

Fig. 5. SAP inhibits PD-1 functions. (*A*) Freshly isolated human CD3$^+$ T cells were transfected with nontargeting control siRNA or siRNA targeting SAP. (*B–D*) Freshly isolated human CD3$^+$ T cells were transfected with a plasmid directing expression of different levels of SAP–GFP (low SAP, 0.4 μg DNA per plate; high SAP, 4 μg DNA per plate) or a control null plasmid. After 24 h, the cells were stimulated with magnetic beads coated with anti-CD3 or anti-CD3+PDL2 for an additional 24 h. At this time, cells were tested for GFP and for CD69 expression by FACS analysis (*B* and *D*), and medium was collected for IL-2 measurements (ELISA) (*A* and *C*). MFI, mean fluorescence intensity. (*E* and *F*) Jurkat T cells, stably transfected with shRNA targeting SAP (KD; knockdown) or a plasmid directing expression of SAP (OE; overexpression) were stimulated as indicated, and medium was collected for IFN-γ while cells were subjected to an adhesion assay using fibronectin-coated wells. Percentage of adhesion was calculated based on input fluorescence. (*G*) Freshly isolated human CD3$^+$ T cells from healthy controls or from XLP patients were stimulated with magnetic beads coated as indicated for 48 h. Medium was harvested, and IL-2 levels were measured with ELISA. (*H*) Freshly isolated human CD3$^+$ T cells from healthy controls or from XLP patients were stimulated with magnetic beads coated as indicated, and cell proliferation was monitored using the MTS assay. Values are expressed as the increase in OD compared with day 0. (*I*) Freshly isolated mouse CD3$^+$ T cells from WT controls or from SAP-deficient mice were stimulated with magnetic beads coated as indicated for 48 h. Medium was harvested, and IL-2 levels were measured with ELISA. (*J*) Freshly isolated mouse CD3$^+$ T cells from WT controls or from SAP-deficient mice were stimulated with magnetic beads coated as indicated, and cell proliferation was monitored using the MTS assay. Values are expressed as the increase in OD compared with day 0. Data are presented as mean ± SEM; asterisks represent significant differences, between the denoted condition and the anti-CD3–treated cells in *A* and *C–F* or between the denoted group and the anti-CD3+28–treated cells in *G–J*; $*P < 0.05$, $**P < 0.01$, $***P < 0.001$, unpaired *t* test; $n = 3$.

suggesting that SAP is a negative regulator of PD-1 functions. Importantly, PD-1 expression levels were maintained at equivalent levels in XLP patients and controls (Fig. S7*E*). Similar to XLP patients, T lymphocytes from SAP-deficient mice had an increased response to PD-1 activation, as demonstrated by a further reduction of IL-2 secretion and cellular proliferation (Fig. 5 *I* and *J*).

SAP Expression Levels Inversely Correlate with PD-1 Signaling in Purified T Cell Subsets. To test whether different expression levels of SAP affect PD-1 function in a physiologic setting, we first separated CD4$^+$ T cells into the following subsets (based on different stages of antigen experience): naive T cells (T_{NAIVE}), central memory T cells (T_{CM}), effector memory T cells (T_{EM}), and terminally differentiated T cells (T_{EMRA}) (Fig. 6*A*) (32). As expected, PD-1 expression levels differed among these subsets (Fig. 6*B* and Fig. S8 for CD8$^+$ T cells). To analyze PD-1 signaling, we measured phosphorylation levels of tyrosine 142 of the ζ chain of the TCR complex (pCD3ζ), as the most proximal phosphorylation event in the TCR signaling cascade, which is also dephosphorylated upon PD-1 engagement (24). As expected, pCD3ζ levels increased upon crosslinking with anti-CD3/28 antibodies (Fig. 6*C*, *Left Column*) and decreased when PDL1 was engaged concomitantly (Fig. 6*C*, *Right Column*). Interestingly, increased PD-1 expression levels (Fig. 6*B*) failed to correlate with the effects of PD-1 ligation on TCR signaling in different T cell subsets, as measured by pCD3ζ levels (Fig. 6*D*). By contrast, SAP expression levels positively correlated with antigen experience (Fig. 6*E*) and inversely correlated with the degree of CD3ζ dephosphorylation (Fig. 6*F*), suggesting a role for SAP in inhibiting PD-1 function in T cell subsets. To further support this hypothesis, SAP knockdown in Jurkat T cells resulted in greater reduction of IL-2 levels downstream of PD-1, as measured by intracellular staining (Fig. S9). Collectively, these results suggest that SAP acts as a negative regulator downstream of PD-1 signaling.

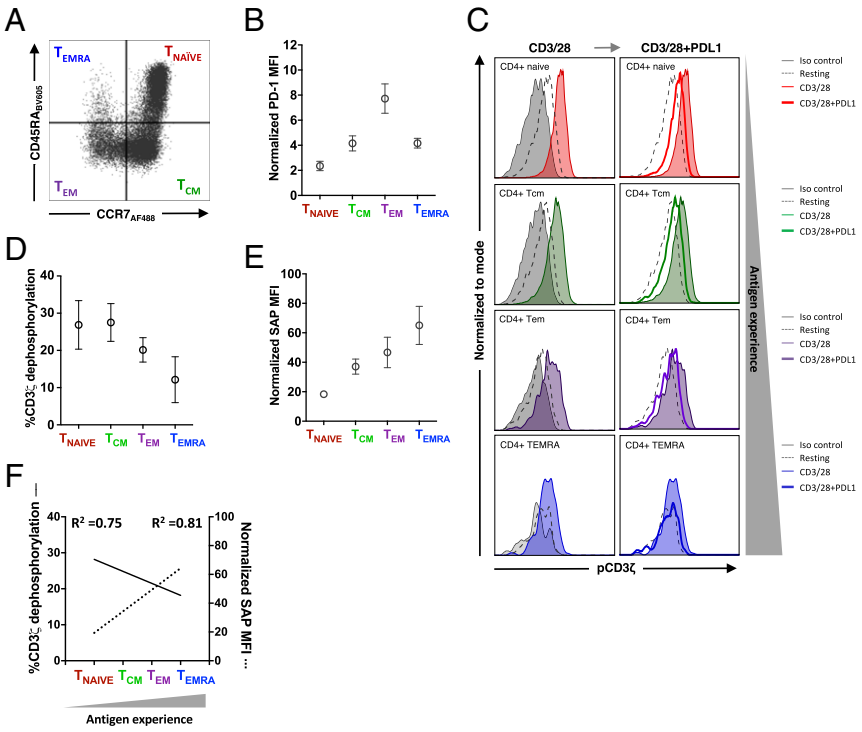

Fig. 6. SAP expression levels inversely correlate with PD-1 signaling in purified T cell subsets. (*A*) Expression of CD45RA and CCR7 by human $CD4^+$ T cells in blood defines four subsets corresponding to T_{NAIVE} ($CD45RA^+CCR7^+$, *Upper Right*), terminal effector (T_{EMRA}; $CD45RA^+CCR7^-$, *Upper Left*), central memory (T_{CM}; $CD45RA^-CCR7^+$, *Lower Right*), and effector memory (T_{EM}; $CD45RA^-CCR7^-$, *Lower Left*) cells. Results shown are from one donor representative of five donors. (*B*) Expression of PD-1 in the different T cell subsets expressed as MFI. (*C*) Representative histograms of pCD3ζ staining: gray histograms, Iso control; colored histogram, crosslinked with anti-CD3/CD28 antibodies; dashed line, resting cells; thick colored line, crosslinked with anti-CD3/28 antibodies in the presence of PDL1. (*D*) CD3ζ dephosphorylation. The MFI of pCD3ζ for each subset was normalized to the MFI of anti-mouse IgG antibody alone. The proportion of CD3ζ dephosphorylation was calculated as the percent change for each subset relative to the crosslinked sample: %CD3ζ dephosphorylation = 100 − [(crosslinked + PDL1/cross-linked) × 100]. (*E*) Expression of SAP in the different T cell subsets expressed as MFI. (*F*) The linear regression of the percentage of CD3ζ dephosphorylation is plotted against the linear regression of SAP expression in the different subsets. Data are presented as mean ± SEM; $*P < 0.05$, unpaired *t* test; $n = 3$.

Discussion

In an attempt to uncover PD-1–interacting partners, we discovered that SAP indirectly inhibits PD-1 function by shielding tyrosine residues from SHP2 activity. Furthermore, while we confirmed previous observations that the PD-1 ITIM and ITSM are both required for maximal SHP2 binding to PD-1, we found that the ITIM is critically required for SHP2 phosphatase activity as well. Collectively, through a series of biochemical investigations and immune-based assays, we have identified SAP as an inhibitor of PD-1 function, and these insights into PD-1 biology might inform future therapeutic strategies targeting the PD-1/SHP2 axis.

Although some of the signaling pathways downstream of PD-1 have been described, many are still poorly understood. Whether the cytoplasmic tail of PD-1 interacts with other downstream effectors is still a matter of debate. SHP2 is recruited to the PD-1 cytoplasmic tail by binding to the phosphorylated PD-1 ITSM following ligand binding and subsequent clustering with the TCR complex (22). However, the role of other phosphatases such as SHP1 and the contribution of the ITIM of PD-1 to downstream signaling are not clear. While Chemnitz et al. (4) reported that PD-1 inhibitory effects were preserved when the ITIM (Y223F), but not the ITSM (Y248F), was mutated, others have suggested that the ITIM is needed for downstream signaling of this pathway (12, 23). In addition, it is not clear what binds to the ITIM, or possibly to the long distal portion of the tail of PD-1.

In this work, we utilized an affinity purification-based approach, using the GST-tagged PD-1 cytoplasmic tail as a bait, coupled with MS analysis, to identify intracellular binders. Focusing on tyrosine-specific interactors, we used relative label-free quantitative analysis to discover candidates that preferentially interacted with the PD-1 WT and not with the phosphodeficient version. Because ITIMs or ITSMs usually recruit adaptor proteins that have SH2 domains, we focused our attention on proteins that were enriched in the PD-1 WT affinity purification and also contained at least one SH2 domain (www.uniprot.org). Further limiting our consideration to immune-related proteins narrowed our list to only three candidates: SHP2, ITK, and SAP (Table 1). Interestingly, SHP1 was not affinity-purified by any of the C-terminal tails. While SHP2 is a known binding partner of PD-1, SAP has never been demonstrated to interact with this receptor. As SAP is known to interact with the ITSMs of the SLAM family receptors, other investigators attempted, although unsuccessfully, to record an association between PD-1 and SAP using 293T cells (4). In our hands, overexpression of SAP impaired the PD-1 inhibitory function by obstructing SHP2 phosphatase activity. This was related to a shielding effect of SAP, whereby SAP protects substrates of SHP2 from its phosphatase activity. The formation of an inhibitory complex that includes SAP, and perhaps additional proteins, to modulate SHP2 activity through an alternative mechanism cannot be excluded.

Several groups have shown that, similar to SAP, other SH2 domains can protect phosphorylated tyrosines from dephosphorylation. Rotin et al. (39) reported that SH2 domains prevented tyrosine dephosphorylation in the context of EGFR. Veillette and coworkers (40) showed that the SH2 domain of LCK protected its C-terminal tail from dephosphorylation. Wills et al. (41) demonstrated a similar protection mediated by the adaptor protein ShcD, and Jadwin (42) presented a method of screening SH2 binding partners based on SH2 protection. However, these papers provide limited physiological relevance. It was recently

found that CD28 is a critical target for PD-1–induced dephosphorylation (23). Our finding that SAP protects CD28 from dephosphorylation by SHP2 further supports the important role of SAP in PD-1 signaling and provides an additional layer of evidence that many SHP2 sites that overlap with SAP binding may actually be shielded from PD-1 signaling, leaving those not shielded by SAP as major functional targets. There are two functional phosphosites in the tail of CD28. The first motif contains the HSDY(p)MNM sequence (CD28 Y173). This motif undergoes tyrosine phosphorylation following the engagement of CD28 and serves as a binding site for the SH2 domain of p85, the regulatory subunit of PI3K. The methionine residue at the +3 position confers specificity for p85 binding, while the asparagine at the +2 position confers additional specificity for the SH2 domain of GRB2 and GADS. A second, more distal motif containing YQPY(p)APP (CD28 Y190) serves as a potential docking site for other effector molecules such as filamin-A, LCK, and FYN. We found that SAP preferentially shields the first motif, and this might result from the serine at −2 position of CD28 Y173, which is considered part of the binding motif of SAP (43). Whether SAP shields the substrates of additional phosphatases, such as CD45, should be explored.

Immunodeficiency and lymphoproliferative disease coexist in XLP patients (34). Similarly, SHP2 is implicated in opposite signaling pathways, as it is involved in mediating lymphoproliferation, being an inducer of the RAS pathway (44), as well as an inhibitor of lymphoproliferation and other lymphocyte functions as a mediator of the PD-1 pathway. Hence, the function of SAP as an inhibitor of SHP2 can explain the pathophysiology of XLP and also points toward SHP2 inhibitors as a possible therapy. Further studies should investigate if SAP shielding is an important determinant of what is observed in vivo and also if it is an important determinant of the XLP phenotype.

The physiological role of SAP in dampening PD-1 responses is less clear, but it is likely to play a role in chronically activated and autoimmune T cells that express high levels of PD-1 but are not inhibited. Indeed, we show here that an increase in SAP expression in antigen-experienced T cell subsets correlated with reduced PD-1 signaling. As PD-1 was shown to have a unique role in germinal centers (45), it would be of interest to study PD-1 and SAP biochemistry and kinetics in additional subsets of lymphocytes, such as regulatory T cells and T follicular helper cells.

SHP2 interacts with the ITSM of PD-1, but the contribution of the ITIM to this system is not clear. We observed a partial reduction in SHP2 binding to PD-1 when the ITIM was mutated. In addition, it is established that SHP2 contains two SH2 domains and that it is fully active when both sites are occupied simultaneously by two adjacent phosphotyrosines (29, 30). In agreement with this model, we found that the enzymatic activity of SHP2 was reduced when either the ITIM or the ITSM was mutated, implying that the ITIM is required for optimal binding of SHP2 to PD-1, SHP2 enzymatic activity, and overall PD-1 function. Recent work by Hui et al. (23) has demonstrated that both the ITIM (Y223) and ITSM (Y248) of PD-1 are involved in SHP2 recruitment. However, while we confirm this work by showing that the ITIM is hardly required for SHP2 recruitment, we observe that a mutation in the ITIM alone completely abolishes SHP2 activity and PD-1 function, and that this discrepancy can be explained by the two-step activation model in which the first step involves recruitment to the ITSM without activation (because of the autoinhibited conformation of SHP2), and SHP2 becomes active only when there is binding of the second SH2 to the ITIM (second step) (Fig. 2*F*).

In the past decade, cancer immunotherapy has become an important arm of cancer treatment, and inhibition of the PD-1 pathway is one of the main avenues of this arm. Biomarkers for anti–PD-1 responders are actively pursued, and our finding implies that interpatient differences in SAP levels, as previously observed in lupus (46), might be relevant to the anti–PD-1 response. In addition, PD-1 ligands are being considered for the treatment of autoimmune diseases (8), and new and potent SHP2 inhibitors were demonstrated to be effective in preclinical studies in tumor models (35). Thus, the newly discovered binding partners of the PD-1 cytoplasmic tail presented in this study hold great potential as therapeutic targets.

Materials and Methods

Additional information regarding the materials and methods is provided in *SI Materials and Methods*.

Transfection and Stimulation. Constructs were introduced into the cells by nucleofection (Lonza) with an efficiency of 50–70%. Cells were stimulated at a 1:3 ratio with magnetic beads (3×10^6 beads per well) (Invitrogen) conjugated with anti-CD3 (UCHT1) (R&D) and IgG1 (R&D) or with anti-CD3 and PDL2-IgG1 (R&D).

Recombinant Proteins. Recombinant peptides were synthesized by GenScript.

DNA Constructs. pMSCV-PD-1-YFP was a gift from James Allison (MD Anderson Cancer Center, Houston, TX). pMSCV-SHP2-flag and pMSCV-null were previously described (47).

Generating Stable Knockdown Jurkat T Cells. SAP was stably knocked down in Jurkat T cells by RNAi using Mission shRNA plasmids (Sigma).

siRNA for Knockdown in Primary Human T-Cells. SMARTpool ON-TARGETplus SH2D1A (SAP), SHP2, and nontargeting control siRNA (Dharmacon) were used according to the manufacturer's instruction.

Cytokine Analysis. Human and mouse IL-2 and IFN-γ ELISA kits (BioLegend) were used according to the manufacturer's protocols.

Cell Proliferation Assay. The cell proliferation assay was performed using tetrazolium compound-based CellTiter 96 AQueous One Solution Cell Proliferation (MTS) assay (Promega).

Immunoprecipitation and Affinity Enrichment. Cell lysates were mixed with anti-GFP monoclonal antibody coupled to agarose beads to enrich GFP-tagged proteins according to the manufacturer's protocols. Pull-down lysates were separated by Tris-glycine PAGE, transferred to nitrocellulose filters, and visualized as described (3). Bacterial expression vectors were used to transform competent BL21 *Escherichia coli* cells. Recombinant protein immobilization on glutathione Sepharose beads (Thermo Scientific), binding assays, and analyses of bound proteins were conducted as described (48).

Phosphatase Activity. To determine kinetic parameters, a fixed amount of purified GST–WT SHP2 catalytic domain was incubated with variable concentrations of substrates (GenScript) in PTP assay buffer (Phosphatase Assay Kit; Upstate 17-313). Phosphatase release was quantified by adding Malachite Green (Malachite Green Phosphatase Detection Kit; R&D DY996).

Flow Cytometry. T cells were studied using a FACSCalibur system (BD) and an LSR II flow cytometer (BD) and were analyzed using FlowJo software.

Static Adhesion Assay. Static T cell adhesion to fibronectin-coated plates was performed as reported (49).

LC-MS/MS. The samples were digested in gel and analyzed on LC-MS as in ref. 50 with modifications as described in *SI Materials and Methods*. The MS/MS spectra were searched against the UniProt Human reference proteome database (downloaded 2016 25 February) (51), with WT and phosphor-impaired GST–PD1 sequences inserted into the database, using SEQUEST within Proteome Discoverer. Database queries to sort for SH2-containing proteins and immune-related proteins are described in detail in *SI Materials and Methods*.

XLP Patients and Healthy Controls. The study was approved by the Institutional Review Boards at The Children's Hospital of Philadelphia and New York University School of Medicine. The patients and healthy human controls provided informed consent for immunologic studies.

Mice. WT C57/Bl6 male mice or SAP-knockout mice (B6.129S6-Sh2d1a^{tm1Pls}/J; The Jackson Laboratory were used) at 6–12 wk of age. Animal studies were

approved by the New York University Institutional Animal Care and Use Committee.

Statistics. Values are reported as mean ± SEM. Statistical analyses were performed using Student's *t* test and ANOVA analysis. All statistical analyses were performed using GraphPad Prism (version 6.0).

ACKNOWLEDGMENTS. We thank the Proteomics core, Mark R. Philips, Ryohei Tsutsumi, Eva Hernandez, Edward A. Fisher, Gregg J. Silverman, and Judith Goldberg (all of New York University), James P. Allison (MD Anderson Cancer Center), David Rubinsztein (Cambridge Institute of Medical Research), and Zaid Jian and Christian Wysocki (University of Texas Southwestern Medical Center) for critical advice and reagents. The project was funded by NIH Grants 1R01AI125640-01 and R01CA49152, the Rheumatology Research Foundation, the Hirschl Trust, and the Colton Family Scholarship Program. Cell sorting/flow cytometric technologies were provided by the New York University cytometry and cell-sorting laboratory supported in part by NIH/National Cancer Institute (NCI) Grant P30CA016087. MS experiments and data analysis were supported in part by New York University School of Medicine and by Laura and Isaac Perlmutter Cancer Center Support Grant P30CA016087 from the NCI.

1. Nishimura H, Nose M, Hiai H, Minato N, Honjo T (1999) Development of lupus-like autoimmune diseases by disruption of the PD-1 gene encoding an ITIM motif-carrying immunoreceptor. *Immunity* 11:141–151.
2. Nishimura H, et al. (2001) Autoimmune dilated cardiomyopathy in PD-1 receptor-deficient mice. *Science* 291:319–322.
3. Azoulay-Alfaguter I, Strazza M, Pedoeem A, Mor A (2015) The coreceptor programmed death 1 inhibits T-cell adhesion by regulating Rap1. *J Allergy Clin Immunol* 135:564–567.
4. Chemnitz JM, Parry RV, Nichols KE, June CH, Riley JL (2004) SHP-1 and SHP-2 associate with immunoreceptor tyrosine-based switch motif of programmed death 1 upon primary human T cell stimulation, but only receptor ligation prevents T cell activation. *J Immunol* 173:945–954.
5. Patsoukis N, et al. (2012) Selective effects of PD-1 on Akt and Ras pathways regulate molecular components of the cell cycle and inhibit T cell proliferation. *Sci Signal* 5:ra46.
6. Barber DL, et al. (2006) Restoring function in exhausted CD8 T cells during chronic viral infection. *Nature* 439:682–687.
7. Paterson AM, et al. (2011) The programmed death-1 ligand 1:B7-1 pathway restrains diabetogenic effector T cells in vivo. *J Immunol* 187:1097–1105.
8. Raptopoulou AP, et al. (2010) The programmed death 1/programmed death ligand 1 inhibitory pathway is up-regulated in rheumatoid synovium and regulates peripheral T cell responses in human and murine arthritis. *Arthritis Rheum* 62:1870–1880.
9. Zhang X, et al. (2004) Structural and functional analysis of the costimulatory receptor programmed death-1. *Immunity* 20:337–347.
10. Agata Y, et al. (1996) Expression of the PD-1 antigen on the surface of stimulated mouse T and B lymphocytes. *Int Immunol* 8:765–772.
11. Keir ME, Butte MJ, Freeman GJ, Sharpe AH (2008) PD-1 and its ligands in tolerance and immunity. *Annu Rev Immunol* 26:677–704.
12. Kleffel S, et al. (2015) Melanoma cell-intrinsic PD-1 receptor functions promote tumor growth. *Cell* 162:1242–1256.
13. Dong H, Zhu G, Tamada K, Chen L (1999) B7-H1, a third member of the B7 family, co-stimulates T-cell proliferation and interleukin-10 secretion. *Nat Med* 5:1365–1369.
14. Freeman GJ, et al. (2000) Engagement of the PD-1 immunoinhibitory receptor by a novel B7 family member leads to negative regulation of lymphocyte activation. *J Exp Med* 192:1027–1034.
15. Latchman Y, et al. (2001) PD-L2 is a second ligand for PD-1 and inhibits T cell activation. *Nat Immunol* 2:261–268.
16. Tseng SY, et al. (2001) B7-DC, a new dendritic cell molecule with potent costimulatory properties for T cells. *J Exp Med* 193:839–846.
17. Couzin-Frankel J (2013) Breakthrough of the year 2013. Cancer immunotherapy. *Science* 342:1432–1433.
18. Tumeh PC, et al. (2014) PD-1 blockade induces responses by inhibiting adaptive immune resistance. *Nature* 515:568–571.
19. Zaretsky JM, et al. (2016) Mutations associated with acquired resistance to PD-1 blockade in melanoma. *N Engl J Med* 375:819–829.
20. Hofmann L, et al. (2016) Cutaneous, gastrointestinal, hepatic, endocrine, and renal side-effects of anti-PD-1 therapy. *Eur J Cancer* 60:190–209.
21. Pentcheva-Hoang T, Chen L, Pardoll DM, Allison JP (2007) Programmed death-1 concentration at the immunological synapse is determined by ligand affinity and availability. *Proc Natl Acad Sci USA* 104:17765–17770.
22. Yokosuka T, et al. (2012) Programmed cell death 1 forms negative costimulatory microclusters that directly inhibit T cell receptor signaling by recruiting phosphatase SHP2. *J Exp Med* 209:1201–1217.
23. Hui E, et al. (2017) T cell costimulatory receptor CD28 is a primary target for PD-1-mediated inhibition. *Science* 355:1428–1433.
24. Sheppard KA, et al. (2004) PD-1 inhibits T-cell receptor induced phosphorylation of the ZAP70/CD3zeta signalosome and downstream signaling to PKCtheta. *FEBS Lett* 574:37–41.
25. Okazaki T, Maeda A, Nishimura H, Kurosaki T, Honjo T (2001) PD-1 immunoreceptor inhibits B cell receptor-mediated signaling by recruiting src homology 2-domain-containing tyrosine phosphatase 2 to phosphotyrosine. *Proc Natl Acad Sci USA* 98:13866–13871.
26. Tian R, et al. (2015) Combinatorial proteomic analysis of intercellular signaling applied to the CD28 T-cell costimulatory receptor. *Proc Natl Acad Sci USA* 112:E1594–E1603.
27. Babu M, et al. (2012) Interaction landscape of membrane-protein complexes in Saccharomyces cerevisiae. *Nature* 489:585–589.
28. Szklarczyk D, et al. (2015) STRING v10: Protein-protein interaction networks, integrated over the tree of life. *Nucleic Acids Res* 43:D447–D452.
29. Pluskey S, Wandless TJ, Walsh CT, Shoelson SE (1995) Potent stimulation of SH-PTP2 phosphatase activity by simultaneous occupancy of both SH2 domains. *J Biol Chem* 270:2897–2900.
30. Sun J, et al. (2013) Antagonism between binding site affinity and conformational dynamics tunes alternative cis-interactions within Shp2. *Nat Commun* 4:2037.
31. Veillette A (2010) SLAM-family receptors: Immune regulators with or without SAP-family adaptors. *Cold Spring Harb Perspect Biol* 2:a002469.
32. Proust R, Bertoglio J, Gesbert F (2012) The adaptor protein SAP directly associates with CD3ζ chain and regulates T cell receptor signaling. *PLoS One* 7:e43200.
33. Sayos J, et al. (1998) The X-linked lymphoproliferative-disease gene product SAP regulates signals induced through the co-receptor SLAM. *Nature* 395:462–469.
34. Filipovich AH, Zhang K, Snow AL, Marsh RA (2010) X-linked lymphoproliferative syndromes: Brothers or distant cousins? *Blood* 116:3398–3408.
35. Chen YN, et al. (2016) Allosteric inhibition of SHP2 phosphatase inhibits cancers driven by receptor tyrosine kinases. *Nature* 535:148–152.
36. Mercan F, Bennett AM (2010) Analysis of protein tyrosine phosphatases and substrates. *Curr Protoc Mol Biol* Chapter 18:Unit 18.16.
37. Dar A, Wu D, Lee N, Shibata E, Dutta A (2014) 14-3-3 proteins play a role in the cell cycle by shielding cdt2 from ubiquitin-mediated degradation. *Mol Cell Biol* 34:4049–4061.
38. Isakov N, Altman A (2012) PKC-theta-mediated signal delivery from the TCR/CD28 surface receptors. *Front Immunol* 3:273.
39. Rotin D, et al. (1992) SH2 domains prevent tyrosine dephosphorylation of the EGF receptor: Identification of Tyr992 as the high-affinity binding site for SH2 domains of phospholipase C gamma. *EMBO J* 11:559–567.
40. Gervais FG, Chow LM, Lee JM, Branton PE, Veillette A (1993) The SH2 domain is required for stable phosphorylation of p56lck at tyrosine 505, the negative regulatory site. *Mol Cell Biol* 13:7112–7121.
41. Wills MK, Tong J, Tremblay SL, Moran MF, Jones N (2014) The ShcD signaling adaptor facilitates ligand-independent phosphorylation of the EGF receptor. *Mol Biol Cell* 25:739–752.
42. Jadwin JA (2017) SH2 binding site protection assay: A method for identification of SH2 domain interaction partners by exploiting SH2 mediated phosphosite protection. *Methods Mol Biol* 1555:477–492.
43. Hwang PM, et al. (2002) A "three-pronged" binding mechanism for the SAP/SH2D1A SH2 domain: Structural basis and relevance to the XLP syndrome. *EMBO J* 21:314–323.
44. Zhang SQ, et al. (2004) Shp2 regulates SRC family kinase activity and Ras/Erk activation by controlling Csk recruitment. *Mol Cell* 13:341–355.
45. Good-Jacobson KL, et al. (2010) PD-1 regulates germinal center B cell survival and the formation and affinity of long-lived plasma cells. *Nat Immunol* 11:535–542.
46. Furukawa H, et al. (2013) Association of a single nucleotide polymorphism in the SH2D1A intronic region with systemic lupus erythematosus. *Lupus* 22:497–503.
47. Mohi MG, et al. (2005) Prognostic, therapeutic, and mechanistic implications of a mouse model of leukemia evoked by Shp2 (PTPN11) mutations. *Cancer Cell* 7:179–191.
48. Li Y, et al. (2004) SPAK kinase is a substrate and target of PKCtheta in T-cell receptor-induced AP-1 activation pathway. *EMBO J* 23:1112–1122.
49. Strazza M, Azoulay-Alfaguter I, Pedoeem A, Mor A (2014) Static adhesion assay for the study of integrin activation in T lymphocytes. *J Vis Exp* e51646.
50. Drummond ES, Nayak S, Ueberheide B, Wisniewski T (2015) Proteomic analysis of neurons microdissected from formalin-fixed, paraffin-embedded Alzheimer's disease brain tissue. *Sci Rep* 5:15456.
51. UniProt Consortium (2015) UniProt: A hub for protein information. *Nucleic Acids Res* 43:D204–D212.
52. Motenko H, Neuhauser SB, O'Keefe M, Richardson JE (2015) MouseMine: A new data warehouse for MGI. *Mamm Genome* 26:325–330.
53. Berger AH, et al. (2016) High-throughput phenotyping of lung cancer somatic mutations. *Cancer Cell* 30:214–228.